

# Intrusion of summer Alaskan Coastal Water in the western Arctic Ocean from 1999 to 2019: insights into interannual trends and driving mechanism

Xinyuan Lv<sup>1</sup> and Na Liu<sup>2</sup>

<sup>1</sup>P.R.China Ministry of Natural Resources(MNR) First Institute of Oceanography

<sup>2</sup>The First Institute of Oceanography,SOA, China

November 23, 2022

## Abstract

This work is a study of the interannual variability of Alaskan Coastal Water (ACW) supplied into the Arctic Ocean during the summer season. Based on hydrological data obtained during ten Chinese National Arctic Research Expeditions conducted in the summer from 1999 to 2019, the expansion of area, volume, thickness, and heat content of ACW in the southern Chukchi Sea and northern Bering Sea have been calculated for the first time, demonstrating the presence of substantial interannual variability. From 1999 to 2019, in general, each of the fundamental parameters showed two stages, namely 1999-2008 and 2010-2019, with the latter being at a higher value than the former. We repeatedly surveyed meridional hydrographic/velocity sections in the vicinity of the Bering Strait to verify that the changes in the water mass flowing into the strait are the main factors affecting water parameters in both the northern Bering Strait and the southern Chukchi Sea.

1     **Intrusion of summer Alaskan Coastal Water in the western Arctic Ocean**  
2     **from 1999 to 2019: insights into interannual trends and driving mechanism**

3     **Xinyuan Lv<sup>1,2</sup> and Na Liu<sup>1,2\*</sup>**

4     <sup>1</sup>Key Laboratory of Marine Science and Numerical Modeling, Ministry of Natural  
5     Resources, Qingdao, China.

6     <sup>2</sup>Qingdao National Laboratory for Marine Science and Technology, Qingdao, China.

7     Corresponding author: Na Liu ([liun@fio.org.cn](mailto:liun@fio.org.cn))

8     **Key Points:**

- 9         • Western Arctic Ocean  
10        • Alaskan Coastal Water (ACW)  
11        • Interannual trends

12  
13  
14  
15  
16  
17  
18  
19  
20  
21  
22  
23  
24  
25  
26  
27  
28

29 **Abstract**

30 This work is a study of the interannual variability of Alaskan Coastal Water (ACW)  
31 supplied into the Arctic Ocean during the summer season. Based on hydrological data  
32 obtained during ten Chinese National Arctic Research Expeditions conducted in the  
33 summer from 1999 to 2019, the expansion of area, volume, thickness, and heat content  
34 of ACW in the southern Chukchi Sea and northern Bering Sea have been calculated for  
35 the first time, demonstrating the presence of substantial interannual variability. From  
36 1999 to 2019, in general, each of the fundamental parameters showed two stages,  
37 namely 1999-2008 and 2010-2019, with the latter being at a higher value than the  
38 former. We repeatedly surveyed meridional hydrographic/velocity sections in the  
39 vicinity of the Bering Strait to verify that the changes in the water mass flowing into the  
40 strait are the main factors affecting water parameters in both the northern Bering Strait  
41 and the southern Chukchi Sea.

42 **Plain Language Summary**

43 The Bering Strait is the sole connection between the Pacific and Arctic Oceans.  
44 Alaskan Coastal Water (ACW) is one of the main ocean currents that merge into the  
45 Arctic Ocean through the Bering Strait from the Pacific Ocean. Its basic characteristics  
46 such as temperature and salinity directly affect the freshwater content and heat budget  
47 of the Arctic. Based on the Chinese National Arctic Research Expeditions, it is found  
48 that near the Chukchi Sea, the characteristics of the interannual variation of ACW from  
49 2010 to 2019 are significantly different from that from 1999 to 2008. Further research  
50 shows that this is closely related to the flow into the Bering Strait.

51 **1 Introduction**

52 The seasonally ice-covered Bering and Chukchi Sea shelves are among the  
53 largest continental shelves in the world (Grebmeier et al., 2006). The Bering Strait  
54 Complex (Anadyr Strait, Shpanberg Strait, and Bering Strait) in the northern Bering  
55 Sea and southern Chukchi Sea is the sole connection between the Pacific and Arctic  
56 Oceans. The flow through the Bering Strait is the only oceanic input from the Pacific  
57 into the Arctic Ocean (AO) (Woodgate, 2018).

58 Pacific water inflow through this complex is an important source of heat,  
59 freshwater, nutrients and Pacific fauna into the AO (Woodgate & Aagaard, 2005;  
60 Woodgate et al., 2005; Grebmeier et al., 2006), specifically in the lower layers of the  
61 AO, including in the layer of summer Pacific water. Pacific waters, supplied through  
62 the Bering Strait, form one third of the incoming water volume responsible for the AO  
63 fresh water balance, and are a powerful heat source, which can influence the thickness  
64 and distribution of the sea ice cover (Woodgate & Aagaard, 2005; Makhotina &  
65 Dmitrenkob, 2011). In summertime, the warm water input melts pack ice (Weingartner  
66 et al., 2005) accounting for the greatest interannual variability in Arctic freshwater  
67 input (Johanna et al., 2017). Pacific water also contributes to the stratification of the  
68 water column over large areas of the western Arctic, helping to maintain the upper  
69 halocline (Anderson et al., 2013; Johanna et al., 2017).

70 In order to reach the central Arctic Ocean, Pacific water must first cross the  
71 wide and shallow Chukchi Sea (Johanna et al., 2017). There are three main flow  
72 pathways by which this occurs, dictated largely by the topography of the shelf  
73 (Weingartner et al., 2005): the Alaskan Coastal Water (ACW) on the east, the Bering  
74 Shelf Water (BSW) in the central area, and the Anadyr Water (AW) on the west  
75 (Grebmeier et al., 2006; Yamashita et al., 2019).

76 In this paper, we mainly study the warmer, less saline, low-nutrient ACW, also  
77 known as the Eastern Chukchi Summer Water (ECSW), which flows northward along  
78 the coast of Alaska toward Barrow Canyon and is referred to as the Alaskan Coastal  
79 Current (ACC) in the warm months of the year (Lin et al., 2019). Alaskan coastal water  
80 originates along the coast over the inner shelf in the eastern Bering Sea; it develops  
81 annually from the input of river water and melting ice from western Alaskan rivers and  
82 its temperature increases rapidly through the spring and summer from about 0 to 10 C°  
83 (Eisner et al., 2013). This current is believed to provide ~0.1 Sv of flow, ~1/3 of the  
84 heat and 1/4 of the freshwater fluxes through the strait (Woodgate & Aagaard, 2005;  
85 Woodgate, 2018).

86 The increase in annual mean transport is reflected in correspondingly  
87 significant increases in the annually integrated fluxes of heat and fresh water. In the  
88 present study, we estimate the interannual variability of the ACW in relation to area  
89 expansion, volume, thickness, and heat content. The analysis has been made for the first  
90 time based on summer data obtained from repeated sections set up in the southern  
91 Chukchi Sea and northern Bering Sea (66°N-75°N) in the 1999-2019 period.  
92 Additionally, in order to explain the characteristics of the interannual variation of ACW  
93 entering the Arctic Ocean, we analyzed the volume and heat fluxes from the zonal  
94 section of the southern Bering Strait (172°W-167°W).

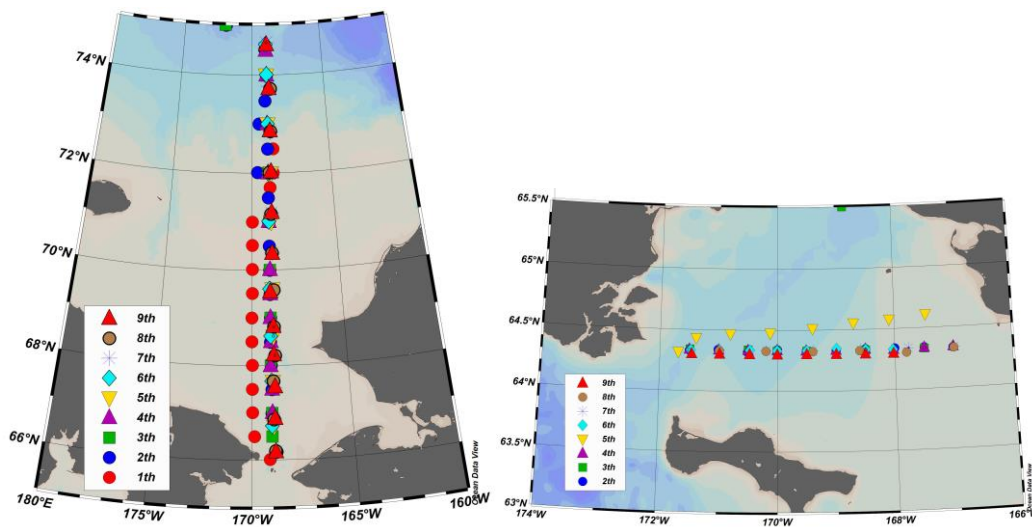
## 95 **2 Data and methods**

### 96 **2.1 Data**

#### 97 **2.1.1 The conductivity-temperature-depth (CTD) Data**

98 From 1999 to 2019, ten repeated zonal hydrographic/velocity sections were set  
99 up in the vicinity of the southern Chukchi Sea and northern Bering Sea during ten  
100 Arctic research expeditions conducted by China. These cruises occurred in the summer,  
101 and even though the timing of each cruise varied among years, it can be considered  
102 quasi-synchronous. We labeled these transects as R and the bottom depth in the study  
103 area was 50 m. The latitude range of these sections was about 66°-75°N, while the  
104 longitude range was 170°-172°W. Additionally, several meridional transects were also  
105 set up during the expeditions at the south end of the Bering strait and across the  
106 northern Bering Sea shelf, and they were labelled either BS, NB or BN. The depth of  
107 every station was also less than 50 m, the latitude range of the sections was  
108 approximately 64.2°-64.6°N, and the longitude range was 167°-171.7°W (Wang et al.,  
109 2020).

110 These two repeated sections both have a distance of less than 1° between  
111 stations. Exact locations of the stations are shown in Figure 1.  
112



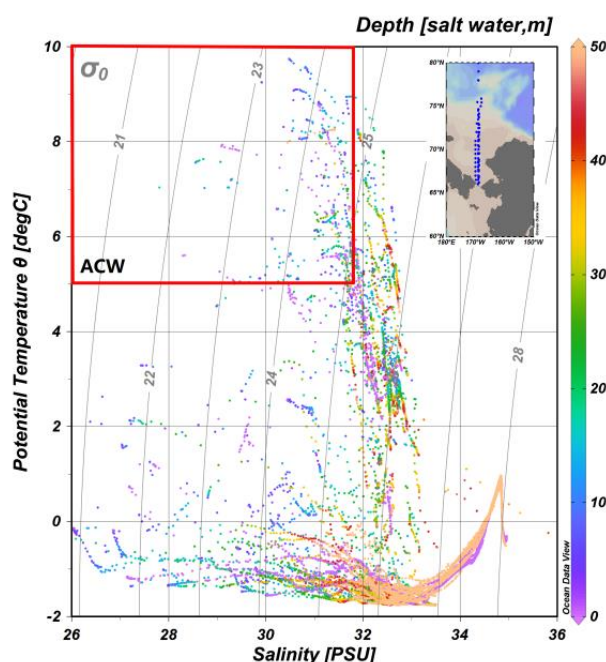
113  
114 **Figure 1.** Distribution of R sections (left) and BS/NB/BN sections (right) collected by  
115 the first nine Chinese National Arctic Research Expeditions.

### 116 2.1.2 HYCOM Reanalysis Data

117 To analyze the volume and heat fluxes and to apply arithmetic corrections (see  
118 section 2.2), we used reanalysis data from the Hybrid Coordinate Ocean Model  
119 (HYCOM). This model includes daily in-situ temperature, sea water salinity, eastward  
120 and northward sea water velocity with a uniform 0.08 degree lat/lon grid between  
121 80.48°S and 80.48°N interpolated to 40 standard z-levels. (Li et al., 2019)

### 122 2.1.3 Water mass identification

123 In the Chukchi Sea, water masses that originate from the Pacific Ocean in the  
124 summer are characterized by temperature (T) and salinity (S) (Nishino et al., 2016).  
125 According to Danielson et al., the ACW temperature is not significantly different in the  
126 two areas of the southern Chukchi Sea and northern Bering Sea, and the ACW salinity  
127 in the northern Bering Sea is within a smaller value. During the midsummer period of  
128 2012 and 2013, the salinity range was roughly 20-32 psu (Danielson et al., 2017). The  
129 combined T/S diagram from data collected during the research expeditions illustrates  
130 the typical summer conditions in the southern Chukchi Sea and northern Bering Sea  
131 (Figure 2) (Gong & Pickart, 2015). To analyze the CTD data, we used ACW definitions  
132 presented in previous studies and that are consistent with our data. However, the precise  
133 definition of each water mass should not be considered invariable because water  
134 properties can change considerably from one year to the next, and, to some extent, from  
135 season to season (Gong & Pickart, 2015). In this paper, ACW is characterized by  
136 potential temperatures  $\geq 5^{\circ}\text{C}$  and by salinities  $\leq 31.8$  psu (Grebmeier et al., 2006; Gong  
137 & Pickart, 2015; Nishino et al., 2016; Danielson et al., 2017).



138

139 **Figure 2.** Temperature-Salinity plot of water masses in the southern Chukchi Sea and  
 140 northern Bering Sea (The area in the red box is the ACW water mass defined in this  
 141 paper, with  $T \geq 5^{\circ}\text{C}$  and  $S \leq 31.8\text{psu}$ )

142 2.2 Methods

143 2.2.1 Calibration of CTD data

144 It was anticipated that, due to the large difference in the time of CTD  
 145 deployment during each expedition, calculations of heat flux, volume flux and heat  
 146 content from datasets would be inaccurate. In order to solve this problem, CTD data  
 147 were calibrated according to the HYCOM reanalysis data, and were corrected for the  
 148 time difference. As far as the R sections are concerned, the data from each expedition  
 149 were all calibrated to August 31 (Table 1), while the data from the BS/NB/BN sections  
 150 were all calibrated to July 26 (Table 2).

151 Firstly, the grid point data closest to the latitude and longitude of each CTD  
 152 station were identified in the HYCOM reanalysis data, then the closest depth was  
 153 located. The average depth near the Bering Strait (that is, near the R and BS sections)  
 154 was 55m, and the available levels in the HYCOM reanalysis data were only 0, 2, 4, 6, 8,  
 155 10, 12, 15, 20, 25, 30, 35, 40, 45 and 50m. Finally, the corresponding two days in the  
 156 HYCOM reanalysis data were subtracted to calculate the difference, and this difference  
 157 was used to correct the CTD data.

158 **Table 1.** Calibration date for each expedition in the R sections

Expedition(time)	Original date	Calibrate date
1th(1999)	August 3	August 31
2th(2003)	July 30	August 31
3th(2008)	August 1	August 31

4th(2010)	July 20	August 31
5th(2012)	September 8	August 31
6th(2014)	July 31	August 31
7th(2016)	September 4	August 31
8th(2017)	Num1: September 10	August 31
	Num1-12: September 22	
9th(2018)	September 7	August 31

159

160

**Table 2.** Calibration date for each expedition in the BS/NB/BN sections

Expedition(time)	Original date	Calibrate date
2th(2003)	July 28	July 26
4th(2010)	July 19	July 26
5th(2012)	July 17	July 26
7th(2016)	September 8	July 26
8th(2017)	September 24	July 26
9th(2018)	September 8	July 26
10 <sup>th</sup> (2019)	August 29	July 26

161

162

### 2.2.2 Ocean Heat Content (OHC)

163

164

165

In this study, the heat content for each station in the R sections was defined as the integrated ocean heat content from a depth of 50 m to sea surface, and it was calculated using the following formula:

166

$$OHC = \int_{-50}^0 4\pi^2 R^2 \rho(T, S) C_p T \cos \phi / 259200 dh$$

167

168

169

170

where R is the radius of the earth, T is the in situ temperature, S is sea water salinity,  $\rho(T, S)$  is the density of seawater, varying with temperature (T) and salinity (S) at depth h,  $C_p$  is the specific heat of seawater,  $\phi$  is the latitude of each station (Ishii & Kimoto, 2009; Wang et al., 2013).

171

172

In addition, CTD temperature and salinity data were interpolated before calculating the heat content, with 0-50 m per meter and 66°N-73°N every 0.1°.

173

### 2.2.3 Thickness, area and volume

174

175

176

177

178

The ACW depth at each CTD site was calculated individually at each station based on the corrected and interpolated data. The average ACW depth at each site was considered as the final thickness value. Because the longitude range between any two stations in the entire R section for each cruise was less than 1° (and data reliability of stations less than 1° apart is very high after interpolation), the longitude range was

179 uniformly set as  $1^\circ$  when calculating the ACW distribution area. The longitude distance  
180 of  $1^\circ$  on latitude A was calculated based on the formula,  $111 \cdot \cos(A)$ . Since the interval  
181 length of a  $1^\circ$  latitude is the same all over the world, the latitude range was converted  
182 into km based on the  $111 \text{ km}/1^\circ$  ratio. Because the Earth is not a perfect sphere, the area  
183 was calculated by averaging the latitude range at the upper and lower latitudes as "long"  
184 and taking the latitude range as "wide". Volume was obtained by multiplying thickness  
185 by area, both derived from of the above calculations.

#### 186 2.2.4 Flux of water masses

187 We used temperature and salinity CTD data (after calibration) and velocity  
188 reanalysis data from the HYCOM to examine the volume flux (V) and heat flux (H)  
189 flowing over the northern Bering Sea shelf from 1999 to 2018. Since the number of  
190 stations and the longitudinal ranges were different each year, we interpolated the data  
191 before calculating the fluxes, with 0-50 m per meter and  $172^\circ\text{W}$ - $167^\circ\text{W}$  every  $0.5^\circ$ . The  
192 volume and heat fluxes (with northward positive direction) (Wang et al., 2020) were  
193 calculated using the following equations:

$$194 \quad V = \sum A_i \cdot v_{ni}$$

$$195 \quad H = \sum C_p \cdot A_i \cdot \rho_i \cdot v_{ni} \cdot T_i$$

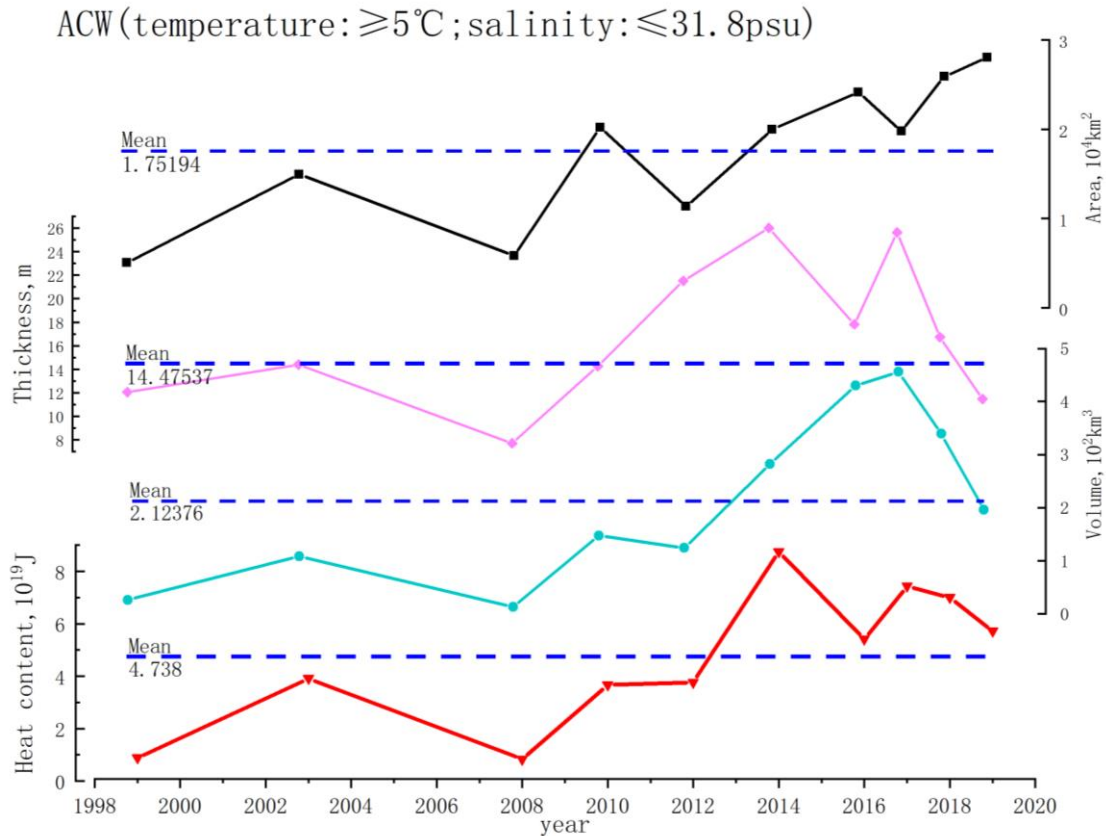
196 where  $A_i$  is the area of i grid,  $v_{ni}$  is the meridional component of the i grid  
197 current in n station,  $C_p$  is the constant pressure specific heat of sea water, the measuring  
198 unit is  $J \cdot \text{kg}^{-1} \cdot ^\circ\text{C}^{-1}$ ,  $\rho_i$  is the density of sea water and  $T_i$  is the temperature.

199

### 200 3 Results

201 The interannual variations in terms of distribution area, thickness, volume and  
202 heat content were divided into two distinct groups: one for years 1999 to 2008  
203 presenting a low level, and the other for years 2010 to 2019, with a relatively high  
204 value.

205 Based on the obtained data on interannual variability, the largest distribution  
206 area of ACW in the southern Chukchi Sea and northern Bering Sea was observed in  
207 2019 exceeding the value of 2017 (when the ACW volume was maximal) by  $0.39 \times 10^4$   
208  $\text{km}^2$  (Figure 3). The minimal values for area and volume were observed both in 1999  
209 and 2008. In 2008 volume was slightly smaller than in 1999, while the distribution area  
210 was slightly smaller in 1999 than in 2008. The overall variation in volume and area was  
211 entirely consistent from 1999 to 2016, while the trend of interannual change from 2016  
212 to 2019 was highly inconsistent. Based on the data for interannual change in thickness  
213 observed in ACW from 2016 to 2019, it is possible to conclude that this variation in  
214 thickness determined the opposite trend variation seen for volume and area during this  
215 time period.



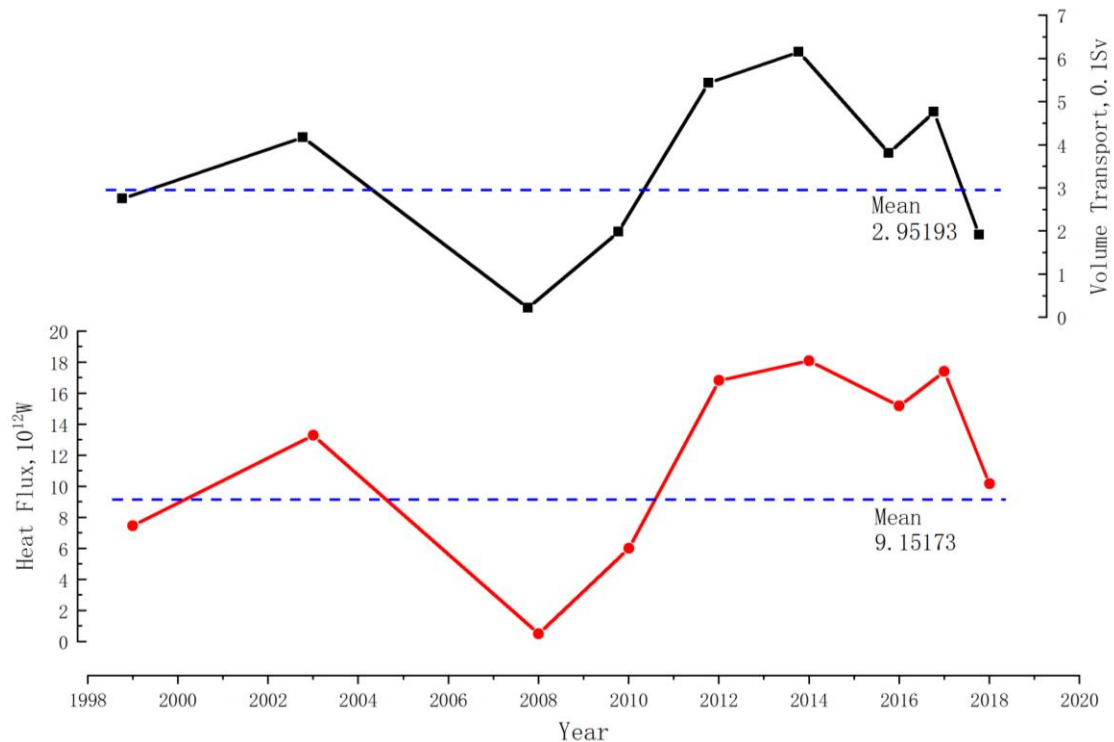
216

217 **Figure 3.** Interannual variability of distribution area (black), thickness (pink), volume  
 218 (blue), and heat content (red) of ACW in the southern Chukchi Sea and northern Bering  
 219 Sea.

220 Data reveal that the average heat content of ACW in the southern Chukchi Sea  
 221 and northern Bering Sea in the 1999-2019 period was  $4.74 \times 10^{19}\text{J}$ . It is worth noting  
 222 that, although the overall change in heat content from 1999 to 2008 remained at a  
 223 relatively low level, the heat content in 2003 increased significantly. Consistent with  
 224 the ACW area and volume, the ACW heat content in 1999 and 2008 was remarkably  
 225 below the climatological data recorded between 1999 and 2020 (Liu et al., 2012). In  
 226 general, the time sequence for ACW parameters from 2008 to 2014 shows a statistically  
 227 significant positive trend (heat content is  $1.98 \times 10^{19} \text{ J/yr}$ ), and in 2014 the heat content  
 228 reached the maximal value ( $8.75 \times 10^{19} \text{ J}$ ). From 2014 to 2019, the values decreased  
 229 though a slight increase was observed between 2016 and 2017. Compared with the  
 230 rising trend seen in the 2008-2014 period, the 2014-2019 trend decreased slowly and  
 231 remained overall above the climatic average.

232 The water properties of the Chukchi Sea are predominantly determined by the  
 233 water mass entering through the Bering Strait (Woodgate et al., 2005; Woodgate,  
 234 2018). In order to analyze interannual variability (Figure 3), we have considered the  
 235 peculiarities of volume and heat transport of ACW through the Bering Strait to the  
 236 Chukchi Sea shelf. In this section, we used the CTD temperature and salinity data (after  
 237 calibration) and velocity reanalysis data from the HYCOM to examine the volume flux  
 238 (V) and heat flux (H) flowing over the northern Bering Sea shelf from 1999 to 2018.

239 The longitude range of the repeated hydrographic/velocity sections was 167°-171.7°W  
 240 (that was for the BN section, NB section and BS section). Since no similar section was  
 241 available for the southern Bering Strait area in 1999, we used the temperature and  
 242 salinity data from the HYCOM reanalysis data to supplement the missing data.



243

244 **Figure 4.** Interannual variability of volume transport (black) and heat flux (red) of  
 245 ACW in the southern Bering Sea.

246 It was possible to conclude that the heat flow through the Bering Strait varies to  
 247 a greater degree, compared to the water flow, and therefore, that it has a greater  
 248 influence on ACW variability in the southern Chukchi Sea and northern Bering Sea. By  
 249 comparing Figure 3 and Figure 4, it is visible that the general heat flux trend of the BS  
 250 section in the southern Bering Strait is consistent with the general heat content trend of  
 251 the R section in the southern Chukchi Sea and northern Bering Sea, although the range  
 252 of change is slightly different in several time periods. For example, the rise in heat flux  
 253 seen from 2010 to 2012 is significant than that seen from 2008 to 2010, while the  
 254 increase in heat content seen from 2008 to 2010 is significant than that seen from 2010  
 255 to 2012. Overall, there is no doubt that the increase in heat flow through the Bering  
 256 Strait leads to the interannual variability of the ACW in the southern Chukchi Sea and  
 257 northern Bering Sea. Similarly, the change in volume transport through the Bering  
 258 Strait can partially explain the interannual change in the ACW volume of the R  
 259 sections. In addition, from 2008 to 2014 there was a continuous upward trend for  
 260 volume transport through the Bering Strait, while there was a slight downward trend in  
 261 the ACW volume between 2010 and 2012. Regardless of the volume or heat fluxes of  
 262 the BS sections, the downward trend observed in the 2003-2008 period is more obvious  
 263 than the upward trend seen between 1999 and 2003. Regardless of the ACW volume or

264 heat content at R sections, the downward trend observed from 2003 to 2008 is almost  
265 the same as the upward trend seen from 1999 to 2003.

#### 266 **4 Conclusions and Discussion**

267 In summary, the expansion of area, volume, thickness, and heat content of  
268 ACW in the southern Chukchi Sea and northern Bering Sea have been calculated for  
269 the first time for the 1999–2019 period; the estimates demonstrate the presence of a  
270 significant interannual variability. All the analyzed parameters show that ACW in the  
271 southern Chukchi Sea and northern Bering Sea from 2010 to 2019 is significantly  
272 strengthened than in the 1999–2008 period. From 2017 to 2019, the ACW entering the  
273 Arctic has gradually become shallower and now shows a clear trend of northward  
274 expansion. In the 1999–2019 period, the innerannual variation of ACW characteristics  
275 was mainly determined by the heat and volume fluxes flowing through the Bering  
276 Strait. The significant interannual variability of distribution area, volume, and heat  
277 content observed in ACW in recent years influences the formation and variability of the  
278 thermohaline structure of the entire Arctic Ocean. We emphasize again that, although  
279 the volume and heat transport through the Bering Strait plays a major role in  
280 determining ACW parameters in the Arctic Ocean, wind force and input from rivers  
281 may also be important.

282 The results indicate that the peculiarities of ACW volume and heat transport  
283 through the Bering Strait to the Chukchi Sea shelf can explain the interannual  
284 variability of the characteristics of ACW, which flows into the Arctic Ocean during the  
285 summer season. However, other processes may also contribute to this variability. For  
286 example, wind strength and direction are important and direct factors influencing the  
287 velocity and flow of water masses; episodic wind-driven upwelling occurs along the  
288 northwestern Alaskan coast, displacing the easternmost branch of the Chukchi  
289 circulation seaward and weakening or reversing the flow that normally takes place  
290 along the coast (Woodgate et al., 2005). In addition, fresh water injection from Alaska's  
291 inland rivers also directly affects the inherent properties of ACW (Eisner et al., 2013).

#### 292 **Data Availability Statement**

293 The CTD data in the southern Chukchi Sea and northern Bering Sea during ten Arctic  
294 research expeditions conducted by China are available at  
295 <https://www.chinare.org.cn/data>. The Hybrid Coordinate Ocean Model (HYCOM) data  
296 used to analyze the volume and heat fluxes and to apply arithmetic corrections were  
297 collected from <https://www.hycom.org/dataserver/gofs-3pt0>.

298

#### 299 **References**

300 Anderson, L.G., Andersson, P.S., Bjork, G., Jones, E.P., Jutterstrom, S., & Wahlstrom,  
301 I. (2013). Source and formation of the upper halocline of the Arctic Ocean. *Journal of*  
302 *Geophysical Research: Oceans*, 118(1): 410–421.  
303 <https://doi.org/10.1029/2012jc008291>

304 Cai, X. J., Jiang, H., Wang, H., & Zuo, J. C. (2013). The relationship between tropical  
305 cyclone in the northwest Pacific and upper ocean heat content. *Acta Oceanologica*  
306 *Sinica (in Chinese)*, 35(3): 28–35. 蔡晓杰, 姜华, 王辉, 左军成. 西北太平洋热带气  
307 旋与上层海洋热含量的关系[J]. 海洋学报, 2013, 35(3): 28-35.

308 Danielson, S. L., Eisner, L., Carol, L., Mordy, C., Sousa, L., & Weingartner, T. J.,  
309 (2017). A comparison between late summer 2012 and 2013 water masses,  
310 macronutrients, and phytoplankton standing crops in the northern Bering and Chukchi  
311 Seas. *Deep-Sea Research II*, 135: 7–26. <http://dx.doi.org/10.1016/j.dsr2.2016.05.024>

312 Eisner, L., Hillgruber, N., Martinson, E., & Maselko, J. (2013). Pelagic fish and  
313 zooplankton species assemblages in relation to water mass characteristics in the  
314 northern Bering and southeast Chukchi seas. *Polar Biology*, 36(1), 87–113.  
315 <https://doi.org/10.1007/s00300-012-1241-0>

316 Gong, D. L., Pickart, R. S. (2015). Summertime circulation in the eastern Chukchi Sea.  
317 *Deep-Sea Research II*, 118: 18–31. <http://dx.doi.org/10.1016/j.dsr2.2015.02.006>

318 Grebmeier, M. J., Cooper, L. W., Feder, H. M., & Sirenko B. K. (2006). Ecosystem  
319 dynamics of the Pacific-influenced Northern Bering and Chukchi Seas in the  
320 Amerasian Arctic. *Progress in Oceanography*, 71, 331–361.  
321 <https://doi.org/10.1016/j.pocean.2006.10.001>

322 Ishii, M., & Kimoto, M. (2009). Reevaluation of historical ocean heat content  
323 variations with time-varying XBT and MBT depth bias corrections. *Journal of*  
324 *Oceanography*, 65(3): 287–299. <https://doi.org/10.1007/s10872-009-0027-7>

325 Johanna, L., Pickart, R. S., Björk, G, & Moore G. W. K. (2017). On the nature and  
326 origin of water masses in Herald Canyon, Chukchi Sea: Synoptic surveys in summer  
327 2004, 2008, and 2009, *Progress in Oceanography*, 159, 99–114.  
328 <https://doi.org/10.1016/j.pocean.2017.09.005>

329 Li, M., Pickart, R., S., Spall, M. A., Weingartner, T. J., Lin, P., Moore, G. W. K., & Qi,  
330 Y. Q. (2019). Circulation of the Chukchi Sea shelfbreak and slope from moored  
331 timeseries. *Progress in Oceanography*, 172: 14–33.  
332 <https://doi.org/10.1016/j.pocean.2019.01.002>

333 Lin, P., Pickart, R. S., McRaven, L. T., Arrigo, K. R., Bahr, F., Lowry, K. E.,  
334 Stockwell, D. A., & Mordy, C. W. (2019). Water mass evolution and circulation of the  
335 northeastern Chukchi Sea in summer: Implications for nutrient distributions. *Journal of*  
336 *Geophysical Research: Oceans*, 124: 4416–4432.  
337 <https://doi.org/10.1029/2019JC015185>

338 Liu, N., Liu, J. P., Zhang, Z. H., Chen, H. X, & Mirong, S. (2012). Short  
339 Communication Is extreme Arctic sea ice anomaly in 2007 a key contributor to severe  
340 January 2008 snowstorm in China? *International Journal of Climatology*, 32: 2081–  
341 2087. <https://doi.org/10.1002/joc.2400>

342 Makhotina, M. S., & Dmitrenkob, I. A. (2011). Interannual Variability of Pacific  
343 Summer Waters in the Arctic Ocean. *Doklady Earth Sciences*, 438(3): 730–732.  
344 <https://doi.org/10.1134/s1028334x11050345>

345 Nishino, S., Kikuchi, T., Fujiwara, A., Hirawake, T., & Aoyama, M. (2016). Water  
346 mass characteristics and their temporal changes in a biological hotspot in the southern  
347 Chukchi Sea. *Biogeosciences*, 13, 2563–2578.  
348 <https://doi.org/10.5194/bg-13-2563-2016>

349 Wang, Y. J., Liu, N., Lin, L. N., He, Y., Kong, B., Zhang, Z. H. (2020). Variation in  
350 water masses on shelf of northern Bering Sea in September 2016–2018. *Marine*  
351 *Geodesy*, 43(3): 285–301. <https://doi.org/10.1080/01490419.2020.1718256>

352 Weingartner, T., Aagaard, K., Woodgate, R., Danielson, S., Sasaki, Y., & Cavalieri, D.  
353 (2005). Circulation on the north central Chukchi Sea shelf. *Deep-Sea Research II*, 52,  
354 3150–3174. <https://doi.org/10.1016/j.dsr2.2005.10.015>

355 Woodgate, R. A. (2018). Increases in the Pacific inflow to the Arctic from 1990 to  
356 2015, and insights into seasonal trends and driving mechanisms from year-round  
357 Bering Strait mooring data. *Progress in Oceanography*, 160, 124–154.  
358 <https://doi.org/10.1016/j.pocean.2017.12.007>

359 Woodgate, R. A., & Aagaard, K. (2005). Revising the Bering Strait freshwater flux into  
360 the Arctic ocean. *Geophysical Research Letters*, 32, L02602.  
361 <https://doi.org/10.1029/2004GL021747>

362 Woodgate, R. A., Aagaard, K., & Weingartner, T. J. (2005). A year in the physical  
363 oceanography of the Chukchi Sea: Moored measurements from autumn 1990-1991.  
364 *Deep-Sea Research II*, 52: 3116–3149. <https://doi.org/10.1016/j.dsr2.2005.10.016>

365 Yamashita, Y., Yagi, Y., Ueno, H., Ooki, A., & Hirawake, T. (2019). Characterization  
366 of the water masses in the shelf region of the Bering and Chukchi Seas with fluorescent  
367 organic matter. *Journal of Geophysical Research: Oceans*, 124: 7545–7556.  
368 <https://doi.org/10.1029/2019jc015476>